PHYSICAL REVIEW B VOLUME 54, NUMBER 14 1 OCTOBER 1996-II

Antiferromagnetic interlayer correlations in annealed $Ni_{80}Fe_{20}$/Ag multilayers

J. A. Borchers, P. M. Gehring, and R. W. Erwin
Reactor Radiation Division, National Institute of Standards and Technology, Gaithersburg, Maryland 20899

J. F. Ankner
Research Reactor Facility, University of Missouri, Columbia, Missouri 65211

C. F. Majkrzak
Reactor Radiation Division, National Institute of Standards and Technology, Gaithersburg, Maryland 20899

T. L. Hylton,* K. R. Coffey, M. A. Parker, and J. K. Howard
IBM Storage Systems Division, 5600 Cottle Road, San Jose, California 95193

(Received 8 March 1996)

Sputtered $Ni_{80}Fe_{20}$/Ag multilayers, annealed post-growth, exhibit giant magnetoresistance (GMR) with pronounced field sensitivity [T. L. Hylton *et al.*, Science **261**, 1021 (1993)]. We have characterized a series of $Ni_{80}Fe_{20}$(20 Å)/Ag(40 Å) multilayers annealed at temperatures ranging from 305 to 335 °C using x-ray and polarized neutron reflectivity techniques. For all of the samples, specular x-ray measurements reveal that the laterally averaged interfaces between the $Ni_{80}Fe_{20}$ and Ag layers are not well defined. The growth-plane morphology of the multilayers, determined from off-specular x-ray diffraction, shows a dependence on annealing temperature. Specular and off-specular polarized neutron reflectivity data indicate that the GMR in the annealed samples does not arise from long-range antiferromagnetic alignment of coherent ferromagnetic sheets, as generally observed in related materials. Instead, annealing promotes the formation of planar ferromagnetic domains of micrometer size within each $Ni_{80}Fe_{20}$ layer that are antiferromagnetically correlated along the growth axis. The length scales of these domains are consistent with a model in which weak dipolar forces dominate the interactions between them. [S0163-1829(96)00337-2]

I. INTRODUCTION

Following the discovery of giant magnetoresistance (GMR) in Fe/Cr multilayers,[1] extensive research efforts have been directed toward the development and optimization of magnetic thin films and multilayers[2] that are suitable for applications as magnetic-field sensors. A dramatic decrease of the resistivity with increasing magnetic field has subsequently been observed in a variety of transition-metal multilayers[3] and generally arises from field-induced alignment of ferromagnetic layers whose spins are otherwise oriented antiparallel across the nonmagnetic interlayers. Changes in the resistivity ($\Delta R/R_{\rm sat}$ where $R_{\rm sat}$ is the resistivity measured in a saturating field and ΔR is the difference between the resistivity in zero field and $R_{\rm sat}$) reported for multilayers such as Co/Cu (Ref. 4) at room temperature and Fe/Cr (Ref. 5) at 4.2 K are approximately 65% and 150%, respectively. Despite the promising magnitude of this effect, few systems are practical for magnetic-recording applications due to the large fields (typically $>$ 500 Oe) required to achieve saturation and overcome interlayer exchange coupling.

In an attempt to satisfy the technological constraints, various groups have designed and constructed thin film systems with novel structural geometries such as granular alloys[6,7] and spin valves.[8] Preparation of the former involves simultaneous deposition of a magnetic and nonmagnetic material followed by post-growth annealing. The GMR observed is pronounced, but the measured saturation fields are again excessive ($>$ 10 kOe), reflecting the strength of the superparamagnetic exchange interaction among the ferromagnetic particles or grains. Spin-valve structures are typically composed of a transition-metal trilayer, such as $Ni_{81}Fe_{19}$/Cu/$Ni_{81}Fe_{19}$, capped with an antiferromagnet (e.g., $Fe_{50}Mn_{50}$) that pins the magnetization of the neighboring ferromagnetic layer.[8] A maximum in the resistivity accompanies the antiparallel alignment of the uncoupled ferromagnetic layers. The saturation fields are small ($\approx$ 200 Oe), but the measured values of $\Delta R/R_{\rm sat}$ generally do not exceed 12–13 %.[9,10]

''Discontinuous'' $Ni_{80}Fe_{20}$/Ag multilayers[11] are among the most promising candidates for low-field sensors because their hybrid structure is specifically designed to overcome many of the geometrical factors that limit the field sensitivity (i.e., change in resistance per unit field) in granular-alloy films.[12] Optimal magnetoresistance (5.3%) with a saturation field of $<$ 100 Oe is achieved by first sputtering alternating layers of $Ni_{80}Fe_{20}$ (i.e., Permalloy) and Ag and then annealing the multilayers post-growth at temperatures near 335 °C for 10 min.[11] (In contrast, we note that similar sputtered samples exhibit resistivity changes as large as 24% after annealing at only 240 °C, but the saturation field exceeds 200 Oe.[13] Samples grown by molecular beam epitaxy[14] show a maximum GMR of 5.6%, which exhibits a pronounced dependence on growth temperature.) The layers are not expected to alloy upon annealing because Permalloy and silver are immiscible. Instead, cross sectional transmission electron microscopy (XTEM) and x-ray diffraction measurements[15] suggest that Ag preferentially seeps into the $Ni_{80}Fe_{20}$ layers at grain boundaries, breaking the ferromagnetic layers into flat ''islands'' or ''pancakes.'' Our specular and off-specular x-ray reflectivity data[16] confirm that subtle changes occur in the in-plane structure and interface morphology upon annealing.

Because the saturation fields measured for our sputtered samples are small, it has been postulated that weak dipolar interactions between the $Ni_{80}Fe_{20}$ particles, rather than interlayer exchange coupling, lead to antiparallel alignment of the ferromagnetic moments across the intervening Ag layers.[11,17] Polarized neutron reflectivity (PNR) provides a means to identify and characterize the magnetic structures of these materials as a function of depth along the growth axis. We have performed specular and off-specular PNR measurements on a series of $[Ni_{80}Fe_{20}(20\ Å)/Ag(40\ Å)]_4$ multilayers, as-deposited and annealed at temperatures ranging from 305 to 335 °C, in order to find evidence of antiferromagnetic or ferromagnetic interlayer coupling. For all of the samples considered, specular reflectivity scans in low fields show *no trace* of either the half-order reflection associated with antiparallel alignment of the layer moments or of the first-order magnetic reflection characteristic of parallel spin alignment. Since the lateral coherence length of the radiation is sufficiently large, PNR effectively averages over many domains within a plane. Therefore, the absence of any magnetic specular scattering in these samples implies that the in-plane magnetic structure consists of many randomly oriented domains.

In principle, quantitative characteristics of the magnetic domains can be obtained from off-specular neutron measurements of diffuse scattering,[18–20] making use of spin polarization to distinguish between structural and magnetic features. We report here the observation of a broad peak in transverse scans (i.e., rocking curves) at the half-order position for the 335 °C annealed multilayer. From the general characteristics and field dependence of this feature, we ascertain that the $Ni_{80}Fe_{20}$ moments order in small in-plane domains that are antialigned across the intervening Ag layers along the growth-axis direction. This peak is absent in data obtained for the as-deposited sample. We thus conclude that the antiferromagnetic correlations in the annealed samples are associated with the resultant GMR. From the width of the off-specular scattering, we estimate the in-plane size of the magnetic domains to be $\approx 1–5\ \mu m$. Calculations of the magnetostatic energy between two flat plates with antiparallel moments demonstrate that dipolar interactions between these domains can account for the antiferromagnetic coupling and the small saturation fields.

II. GROWTH AND BULK PROPERTIES

The multilayers for this study were sputtered onto 1-in.-diameter silicon substrates at ambient temperature in a partial argon atmosphere at a pressure of 3 mTorr. The nominal composition of all four samples is $Ta(100\ Å)/Ag(20\ Å)/[Ni_{80}Fe_{20}(20\ Å)/Ag(40\ Å)]_4/Ni_{80}Fe_{20}(20\ Å)/Ag(20\ Å)/Ta(40\ Å)/SiO_2(700\ Å)/Si$. Following growth, three of the multilayers were annealed for 10 min in an Ar atmosphere at temperatures of 305, 315, and 335 °C, respectively. A more comprehensive description of the deposition and annealing process is provided elsewhere.[11,15]

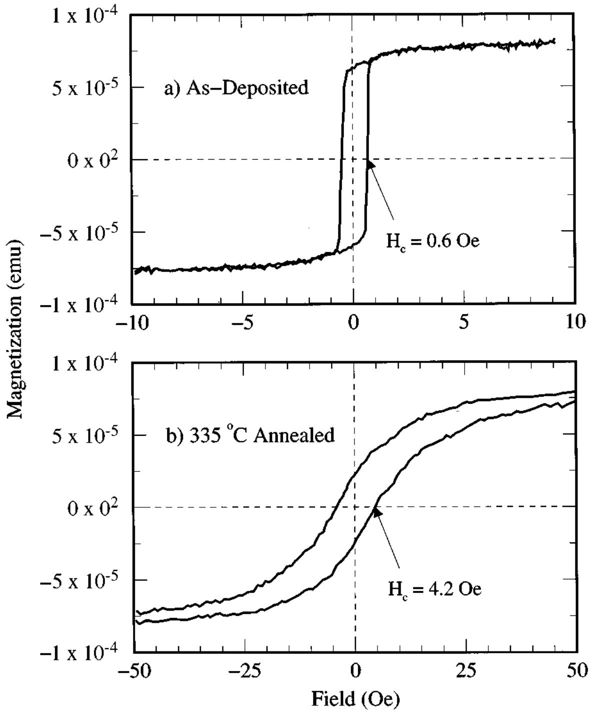

FIG. 1. Room-temperature magnetization as a function of field for the (a) as-deposited and (b) 335 °C annealed samples. Coercive field values H_c corresponding to the demagnetized or zero-magnetization state are designated with arrows.

The bulk magnetic characteristics of these multilayers match those reported previously for a comparable series of samples.[11] Magnetoresistance and magnetization experiments were performed at IBM, San Jose, on smaller, rectangular samples grown and annealed concurrently with the 1-in. wafers. A four-point, in-line contact geometry was used for the measurement of the magnetoresistance with a magnetic field applied in the sample plane perpendicular to the current direction, and a vibrating sample magnetometer was used to measure the bulk magnetization. $\Delta R/R_{sat}$ data obtained for all four samples reveal that a maximum GMR of 4.5% is achieved after annealing at 335 °C, while $\Delta R/R_{sat}$ for the as-deposited sample is smaller than 0.3%, in agreement with values obtained in a related study.[11]

The contrast between the field-dependent magnetization data for the 335 °C annealed and as-deposited samples, plotted in Fig. 1, indicates an evolution of the magnetic structure with annealing temperature. The curve for the as-deposited multilayer resembles that of a simple ferromagnet with a saturation field of approximately 5 Oe and a coercive field H_c of 0.6 Oe. The hysteresis loop for the annealed sample has characteristics more typical of antiferromagnetic interlayer alignment with a saturation field of nearly 50 Oe and $H_c = 4.2$ Oe. However, the exact nature of the magnetic structure in the demagnetized state (i.e., zero-moment state marked with an arrow in Fig. 1) cannot be determined from magnetization data alone. We also note that the field-dependent magnetization for all four samples is essentially isotropic in the film plane.

III. STRUCTURAL CHARACTERIZATION

The structural quality of the multilayers was probed using x-ray reflectometry techniques. We performed these mea-

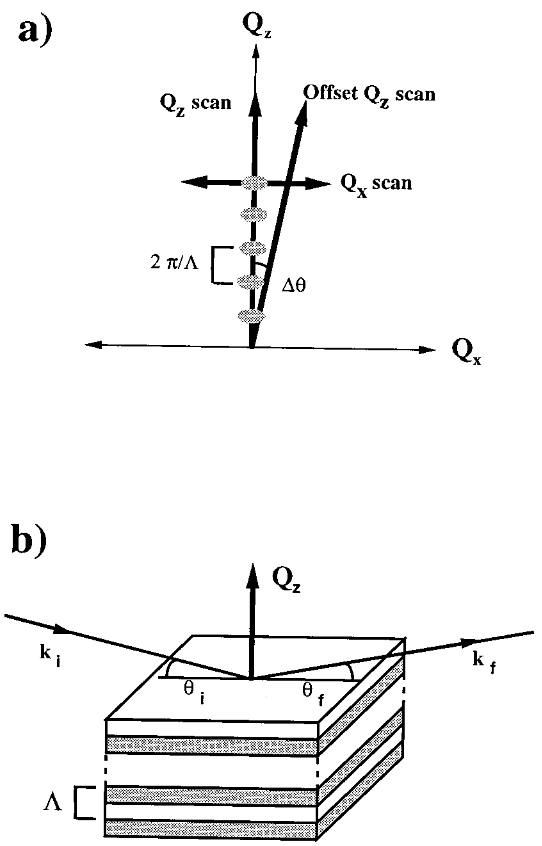

FIG. 2. (a) Schematic diagram of the x-ray and neutron scattering geometry in reciprocal space. Ovals represent the multilayer Bragg reflections separated by $\Delta Q_z = 2\pi/\Lambda$. The heavy arrows designate longitudinal-Q_z, offset-Q_z, and transverse-Q_x scan directions, as marked. (b) Real space representation of scattering from a multilayer where θ_i is the angle of the incident radiation relative to the surface and θ_f is the angle of the scattered radiation.

surements at the National Institute of Standards and Technology (NIST) on a double-axis diffractometer with a graphite analyzer positioned in front of a scintillation detector. A fixed Cu anode source generates radiation of wavelength (λ) 1.541 Å. The horizontal beamwidth at the sample position of approximately 0.05 mm is defined by a vertical slit after the x-ray source, and the intensity in the direction perpendicular to the diffraction plane (y axis) is integrated by the detector.

We have measured the specular and diffuse scattering in reciprocal space using longitudinal-Q_z, offset-Q_z, and transverse-Q_x scan geometries represented schematically in Fig. 2(a). In each case, x rays impinge upon the sample surface at an angle θ_i and are scattered at an angle θ_f as shown in Fig. 2 (b). The magnitude of the wave vector **Q** is defined as $4\pi\sin\theta/\lambda$ where $2\theta = \theta_i + \theta_f$. For longitudinal-$Q_z$ scans along the growth direction (z axis), the incident and exit angles are equal ($\theta_i = \theta_f = \theta$) and incremented together. If the multilayer periodicity is well defined, Bragg reflections will appear at $Q_z = 2\pi n/\Lambda$, where Λ is the bilayer repeat distance and n is an integer. We refer to the resultant data as the *total* reflectivity because both the specular reflectivity from the laterally averaged interfaces and the off-specular reflectivity from the interfacial imperfections contribute to the measured intensity. After subtraction of the off-specular background measured with offset-Q_z scans, these data provide a quantitative gauge of the concentration variation and degree of ‘‘mixing’’ through the multilayer interfaces, but they are not sensitive to the characteristics or length scale of the in-plane features responsible for the interfacial disorder.

Direct measurements of the diffuse scattering via transverse-Q_x and offset-Q_z scans provide a means to determine the length scale of in-plane structural correlations[21,22] and thus can distinguish between short-range disorder resulting from interdiffusion or roughness and long-range disorder resulting from terracing, pinhole formation, or grain boundaries. For transverse scans, the scattering angle 2θ is held constant while θ_i and θ_f are varied equally in opposite directions ($\theta_i + \theta_f =$ const). If Q_x/Q_z is small, these rocking curves approximate Q_x scans in reciprocal space at discrete values of Q_z, as shown in Fig. 2(a). Typically a narrow specular peak, evident at $Q_x = 0$, can be separated from the underlying diffuse scattering which is broad. The width of the diffuse peak is indirectly related to the inverse of the in-plane coherence length as demonstrated by Savage *et al.*[22] In the kinematic limit, a general expression for the diffuse intensity scattered from a single rough surface can be expressed as[21,22]

$$I_{\mathrm{diff}} \propto \frac{e^{-Q_z^2\sigma^2}}{Q_z^2}\int\int dx\,dy\left[e^{Q_z^2 C(x,y)}-1\right]e^{-i(Q_x x+Q_y y)}. \quad (1)$$

The in-plane height-height correlation function $C(x,y)$ is usually assumed to be that for a self-affine fractal surface,[21]

$$C(x,y)=\langle \delta z(0)\,\delta z(x,y)\rangle=\sigma^2\exp\left(-\left[\frac{\sqrt{x^2+y^2}}{\xi}\right]^{2h}\right), \quad (2)$$

where σ is the rms value of the surface roughness, h is the roughness exponent, and ξ is the in-plane correlation length of the roughness.

Offset-Q_z scans are similar to longitudinal-Q_z scans with the sample rotated $\Delta\theta$ from the specular condition ($\theta_i = \theta + \Delta\theta$, $\theta_f = \theta - \Delta\theta$) such that only diffuse intensity is sampled. (We typically chose $\Delta\theta$ equal to 2–3 times the full width at half maximum of the narrow specular peak measured in transverse-Q_x scans at small Q_z.) In reciprocal space [Fig. 2(a)] these Q scans tilt away from the z axis and are thus sensitive to both the in-plane and interlayer correlations between the rough interfaces. The resultant off-specular data are generally subtracted as background from the total reflectivity, but the presence of distinct superlattice peaks in these data is an indication of conformal roughness between interfaces.[23,24]

The total reflectivity relative to the diffuse background is plotted as a function of Q_z for the as-deposited and the 315 °C annealed multilayers in Fig. 3. Superlattice reflections at $Q_z = 2\pi n/\Lambda$, where n is an integer and $\Lambda \approx 60$ Å, are present out to at least second order, but show a rapid decrease in intensity with increasing Q_z. Apparently the interfacial disorder in these multilayers is significant even prior to annealing. For both samples the offset-Q_z scattering is large and has features that mimic those in the total reflectivity data. Finite-size oscillations separated by $\Delta Q_z = 2\pi/D$,

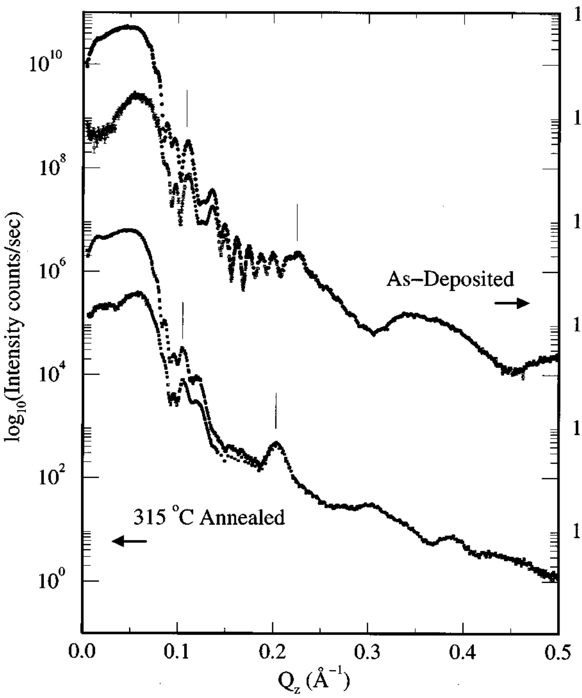

FIG. 3. Total x-ray reflectivity as a function of Q_z measured at room temperature for the as-deposited (shaded circles) and the 315 °C annealed (shaded squares) samples. The diffuse background for the former (open circles) was measured by offsetting the incident angle of the x-rays (θ_i) from $2\theta/2$ by 0.04 °. For the latter, the background (open squares) was measured by offsetting θ_i by 0.033 °. The data for the two samples are vertically displaced by four orders of magnitude for clarity. (The arrows point to the appropriate vertical axis for each sample.) The superlattice reflections for both samples are marked by vertical lines. Clearly the bilayer thicknesses of the multilayers are slightly different, as indicated in Table I.

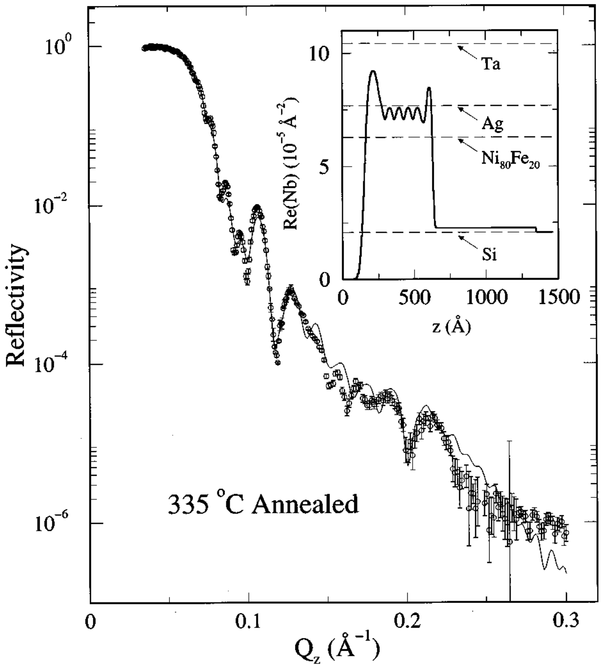

FIG. 4. X-ray reflectivity of the multilayer annealed at 335 °C. The circles correspond to the data and the solid line is the fit. The pronounced feature near $Q_z = 0.106$ Å^{-1} is *not* a superlattice peak. Instead, it is an interference effect from the Ta cap and base layers. The real part of the scattering length density profile, obtained from the fit, is plotted in the inset as a function of depth. The sample has nominal composition Ta(100 Å)/Ag(20Å)/[$Ni_{80}Fe_{20}$(20 Å)/Ag(40 Å)]$_4$/$Ni_{80}Fe_{20}$(20 Å)/Ag(20 Å)/Ta(40 Å)/SiO_2(700 Å)/Si and the topmost Ta layer, which is partially oxidized or degraded, begins at $z = 0$. Dashed lines mark the bulk densities of Ta, Ag, $Ni_{80}Fe_{20}$ and Si.

where $D \approx 480$ Å is the total multilayer thickness, are evident in the offset-Q_z scan for the as-deposited sample (Fig. 3). Constructive interference between the diffuse scattering from the top and bottom surfaces of the multilayer can only be observed if the in-plane interfacial structure is *strongly* correlated or reproduced from one bilayer to the next.[23,24] That superlattice reflections are evident in the offset-Q_z scan for the 315 °C annealed multilayer (Fig. 3) suggests that the roughness is also correlated from bilayer to bilayer in this sample, though the in-plane structures of the Ta base and cap layers probably differ. In other words, the interfaces between the $Ni_{80}Fe_{20}$ and Ag for all of the samples considered are ‘‘sharp’’ over a short length scale.

In Fig. 4, the true specular reflectivity for the 335 °C annealed multilayer, obtained by subtracting the diffuse background from the total reflectivity, is shown as a function of Q_z. Following the subtraction, the specular intensity is negligible for $Q_z > 0.3$ Å^{-1}, as is evident in Fig. 3. To quantify the structural characteristics of the multilayers, we have fit the x-ray data to a dynamical scattering model based upon the one-dimensional wave equation for a stratified medium, taking into account the real and imaginary parts of the scattering length, where the latter is related to the absorption.[25] The fitted curve (solid line in Fig. 4) was generated from the spatial profile of the complex scattering length density. The real part Re(Nb) is shown in the inset of Fig. 4, where N is the number density of the scatterers and b is the scattering length. (For x rays, $Nb = \rho_e r_e$, where ρ_e is the electron density of the material and r_e is the Thomson scattering length or electron radius.) To allow for interfacial diffusion or roughness, the variation of the scattering density through the layer boundaries is represented as an error function with variable full width. Judging from the shape of the interfaces, the $Ni_{80}Fe_{20}$ and Ag layers in the 335 °C annealed sample are *strongly* mixed. Ag atoms are present throughout the nominal $Ni_{80}Fe_{20}$ layers and vice versa. For all four of the multilayers considered, the scattering densities in the center of the nominal $Ni_{80}Fe_{20}$ and Ag layers, listed in Table I, differ from their bulk values. Unfortunately, the analysis is far more sensitive to the characteristics of the high-contrast Ta layers, than to the relative thicknesses and scattering densities of the repeated $Ni_{80}Fe_{20}$ and Ag layers. (Interference from the Ta layers gives rise to the pronounced feature near $Q_z = 0.106$ Å^{-1} in Fig. 4 for the 335 °C annealed sample.) We can state with certainty that the Ta base layer degrades, oxidizes, and/or forms a silicide upon annealing at 335 °C and thus confirm the trend suggested by previous high-angle diffraction studies.[15] Guided by the subsequent neutron reflectivity analysis described in Sec. IV, x-ray fits for the as-deposited[16] and 335 °C annealed samples show that Ag

TABLE I. Structural parameters describing the repeated $Ni_{80}Fe_{20}$ and Ag layers and top Ta and bottom Ta layers in annealed multilayers obtained from the best fits to the specular x-ray reflectivity. Upon fitting, the interfacial full widths for the $Ni_{80}Fe_{20}$ and Ag layers tended to exceed the interlayer thicknesses and were thus constrained to equal the $Ni_{80}Fe_{20}$ thickness. Uncertainties in the layer thicknesses d and real part of the scattering length densities $\mathrm{Re}(Nb)$ were estimated from variations among comparable fits. For comparison the bulk scattering densities for $Ni_{80}Fe_{20}$, Ag, and Ta are 6.28×10^{-5}, 7.67×10^{-5}, and 10.4×10^{-5} Å^{-1}, respectively.

Sample	$Ni_{80}Fe_{20}$		Ag		Ta cap		Ta base	
	d (Å)	$\mathrm{Re}(Nb)$ (10^{-5}Å)	d (Å)	$\mathrm{Re}(Nb)$ (10^{-5}Å)	d (Å)	$\mathrm{Re}(Nb)$ (10^{-5}Å)	d (Å)	$\mathrm{Re}(Nb)$ (10^{-5}Å)
As-dep	24.0 ± 3	6.8 ± 0.2	35.3 ± 2.5	7.5 ± 0.2	100 ± 3	9.4 ± 0.2	39 ± 1	10.1 ± 0.5
305 °C	19.8 ± 3	6.9 ± 0.3	40.9 ± 3	7.3 ± 0.4	102 ± 4	8.8 ± 0.2	48 ± 3	10.1 ± 0.3
315 °C	24.2 ± 3	6.8 ± 0.3	39.2 ± 3	7.4 ± 0.3	99.0 ± 3	8.8 ± 0.2	45.8 ± 1	10.1 ± 0.6
335 °C	23.4 ± 1.5	6.9 ± 0.2	41.8 ± 2	7.6 ± 0.2	95.2 ± 3	9.2 ± 0.2	42.4 ± 2	8.6 ± 0.5

migrates preferentially into the $Ni_{80}Fe_{20}$ layers, possibly through the grain boundaries, though the Ag layer itself remains largely intact.

Most of the structural parameters obtained from the x-ray fits (Table I) show little dependence on annealing temperature outside of their estimated uncertainty range, with the exception of the bilayer spacing. The spacing Λ appears to vary from 59 Å to 65 Å as the annealing temperature is increased to 335 °C, in opposition to the trend reported for Permalloy/Ag multilayers grown by molecular beam epitaxy.[14] This change may be systematic, but we caution that Λ for each sample was only measured after annealing.

Though the specular Q_z reflectivity data indicate that the $Ni_{80}Fe_{20}$ and Ag layers are not distinct in any of the four multilayers considered, it is important to remember that these measurements are only sensitive to the interfacial structure *averaged* across the sample surface. From the offset-Q_z scans described above (Fig. 3), we conclude that the interfacial mixing arises primarily from microscopic structural inhomogeneities within the sample plane that are replicated from one bilayer to the next, rather than from atomic-scale roughness or diffusion. While it is difficult to identify the mechanism responsible for these defects, transverse-Q_x scans provide information about the in-plane correlation length of these features and their dependence on annealing temperature. Figure 5 shows the scattered intensity as a function of Q_x for all four samples measured at $Q_z = 0.213$ Å^{-1} near the second-order superlattice reflection. The absence of resolution-limited specular scattering at $Q_x = 0$ indicates that the peak is principally diffuse in character at this value of Q_z (Fig. 3). Figure 6 demonstrates that the full width at half maximum (FWHM) of the diffuse peak, obtained from fits to a Gaussian or Lorentzian line shape, exhibits an almost quadratic dependence on Q_z for all four of the multilayers considered. (We caution that the fits of the diffuse scattering are not unique because they are sensitive to the choice of background due to the presence of Yoneda scattering[21] at large $|Q_x|$.)

The systematic decrease of the diffuse peak width with increasing annealing temperature, apparent in Fig. 5, is consistently observed in transverse-Q_x data measured at Q_z ranging from 0.057 to 0.285 Å^{-1} (Fig. 6). Assuming that the in-plane structure is perfectly correlated from one multilayer interface to the next, we can crudely characterize the interfaces by comparing the Q_z dependence of the FWHM of the diffuse scattering predicted by Eq. (1) to the Q_z dependence of the widths in Fig. 6. Additional quantitative information is gained by fitting several of the off-specular Q_x scans (e.g., Fig. 5) to Eq. (1). For the as-deposited and 335 °C annealed multilayers, these data are best described by 20 Å $<\sigma<$ 30 Å, which is comparable to the width of the $Ni_{80}Fe_{20}$ interlayers. The resultant ξ values vary between 3.5 and 5.5 μm, implying that the in-plane structures and/or grains are quite elongated. (The range of these estimates could certainly be narrowed by analyzing these data within the context of a dynamical low-angle scattering formalism,[21,26,27] but such a treatment is beyond the scope of this paper. In addition, theories published to date do not describe the Yoneda-like features in multilayer data with sufficient quantitative precision.[18]) The fact that the width of the Q_x scans is smallest for the 335 °C sample (Fig. 6) indicates that the correlation length ξ of the in-plane roughness is largest for this

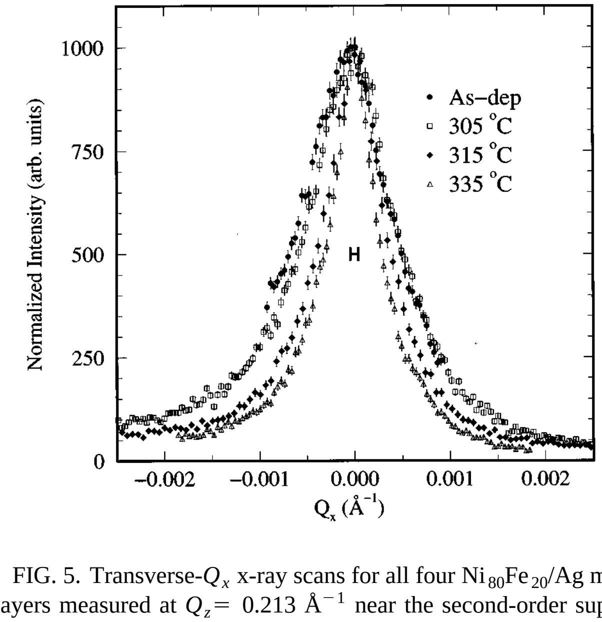

FIG. 5. Transverse-Q_x x-ray scans for all four $Ni_{80}Fe_{20}$/Ag multilayers measured at $Q_z = 0.213$ Å^{-1} near the second-order superlattice reflection. At this Q_z value the intensity is principally diffuse in character. The peak intensities have been scaled to emphasize the dependence of the peak width on annealing temperature and the data have been smoothed by averaging adjacent points. The centered line represents the resolution of the x-ray diffractometer obtained from comparable measurements of a flat Si wafer.

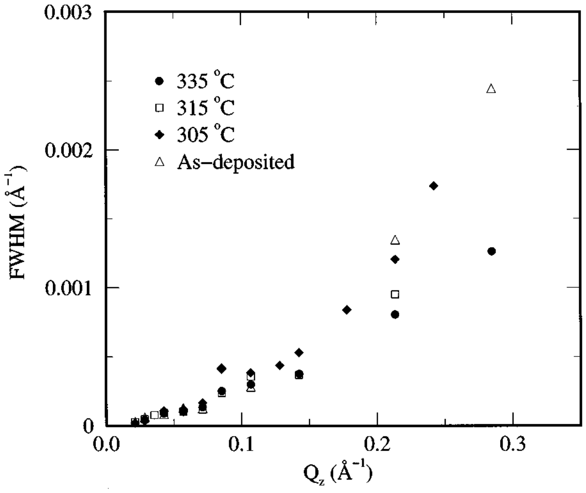

FIG. 6. Q_z dependence of the FWHM of the diffuse scattering component in transverse-Q_x x-ray data for the four multilayers considered. These widths were obtained from fits of the diffuse scattering to a Gaussian or a Lorentzian. Though error bars are not shown for clarity, the error estimates are as large as 10%–15% at high Q_z, due to interference of Yoneda scattering and ambiguities regarding the diffuse lineshape.

multilayer, while σ remains approximately constant. Annealing up to 335 °C thus seems to smooth the surfaces and increase the lateral domain size. The interfaces are ‘‘flatter’’ in annealed samples.

IV. MAGNETIC STRUCTURE DETERMINATION

In analogy to the multilayer structural characterization using x-ray diffraction techniques described in the previous section, the depth-dependent magnetization profile of the samples can be extracted from polarized neutron reflectivity measurements. We obtained these data on the BT-7 reflectometer at the NIST Research Reactor. In the experimental setup,[28] neutrons of wavelength 2.35 Å selected by a pyrolytic graphite (PG) monochromator are incident upon an Fe/Si supermirror which reflects only one of the two neutron spin states. After passing through a spin flipper made of flat Al coils, the neutrons are scattered from the sample through a second spin flipper and then reflected from an analyzing supermirror into a ^{3}He detector. The polarization of the neutrons is maintained by a small guide field ($\gtrsim$ 10 Oe) applied perpendicular to the scattering plane along the entire flight path. In this configuration, we can measure both the non-spin-flip (I_{++} and I_{--}) and spin-flip (I_{+-} and I_{-+}) scattered intensities. The polarizing efficiencies of the front and rear supermirrors are typically 98 ± 1% and 94 ± 1%, while the flipping efficiencies of the front and rear flippers are both 98 ± 1%. To ensure a uniform field environment, we positioned the multilayers in the center of an Al solenoid capable of generating applied fields in the sample plane from -150 to 150 Oe with a precision of about ± 0.1 Oe. Stable saturating fields of $\geqslant$ 250 Oe were obtained by mounting permanent C-magnets near the sample holder.

Using this instrumental configuration, we measured the polarization dependence of both specular and diffuse scattering from all four multilayers as a function of magnetic field. We used the same longitudinal-Q_z, offset-Q_z, and transverse-Q_x scan geometries as in the x-ray experiments [Fig. 2(a)], but the off-specular PNR measurements were more difficult due to inherent limitations in the polarized neutron flux and signal-to-noise ratio. As a result, the offset-Q_z scans show no distinguishing features and are useful only as a gauge of the background relative to the total reflectivity. These results will not be discussed here in any detail.

In order to describe the specular data, the dynamical formalism applicable to the x-ray analysis[25] must be expanded to include the interaction between the spins of the incident neutrons and the sample moments. Detailed expressions for the scattering structure factors are derived elsewhere.[28,29] The general features of the PNR data can most easily be understood within the context of kinematic theory, which is directly applicable only at scattering angles well above the critical angle. For neutrons polarized perpendicular to the scattering wave vector Q_z, the non-spin-flip and spin-flip intensities are described by the following expressions respectively:[28,30]

$$I_{++}\propto\left|\sum_{m}^{M_{\text{tot}}}(b_m+C\mu_m\cos\phi_m)e^{iQ_zz_m}\right|^2,$$

$$I_{--}\propto\left|\sum_{m}^{M_{\text{tot}}}(b_m-C\mu_m\cos\phi_m)e^{iQ_zz_m}\right|^2 \tag{3}$$

and

$$I_{+-}\propto\left|\sum_{m}^{M_{\text{tot}}}C\mu_m\sin\phi_m e^{iQ_zz_m}\right|^2,$$

$$I_{-+}\propto\left|\sum_{m}^{M_{\text{tot}}}-C\mu_m\sin\phi_m e^{iQ_zz_m}\right|^2 \tag{4}$$

where M_{tot} is the total number of atomic planes along the z-axis direction, z_m is the position of the mth atomic plane, and b_m is the average nuclear scattering length of the mth plane. The parameter μ_m is the average in-plane moment of the mth atomic plane, ϕ_m is the average angle between the magnetization and the applied guide field, and C includes a constant equal to 0.27×10^{-12} cm/μ_B multiplied by the Q-dependent magnetic form factor. These equations clearly demonstrate that the difference between the $(++)$ and $(--)$ intensities is related to the component of the sample moment parallel to the field direction, while the spin-flip scattering measures the component of the magnetization perpendicular to the applied field. By fitting all four cross sections simultaneously, one can extract the magnitude and orientation of the moment projection in the growth plane as a function of depth, along with structural information complementary to that obtained from refinement of the specular x-ray data (Fig. 4).

In a saturating field of 250 Oe, specular reflectivity scans for all four of the samples are similar to that shown in Fig. 7 for the 335 °C annealed sample. These data have been corrected for both diffuse background contributions and efficiencies of the polarizing elements using procedures described elsewhere.[28] (We note that we measured all four polarization cross sections over the entire Q_z range shown,

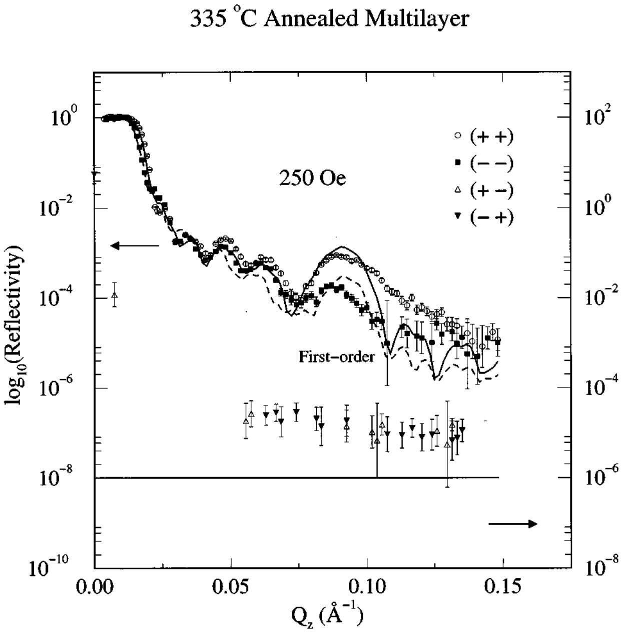

FIG. 7. Polarized neutron reflectivity for the 335 °C annealed sample in a saturating field of 250 Oe. The circles and squares designate the $(++)$ and $(--)$ non-spin-flip cross sections, respectively, and the triangles and inverted triangles mark the $(+-)$ and $(-+)$ spin-flip cross sections, which are vertically offset by two orders of magnitude for clarity. (The arrows point to the appropriate vertical axis for each set of cross sections.) The solid and dashed lines correspond to a fit to the data.

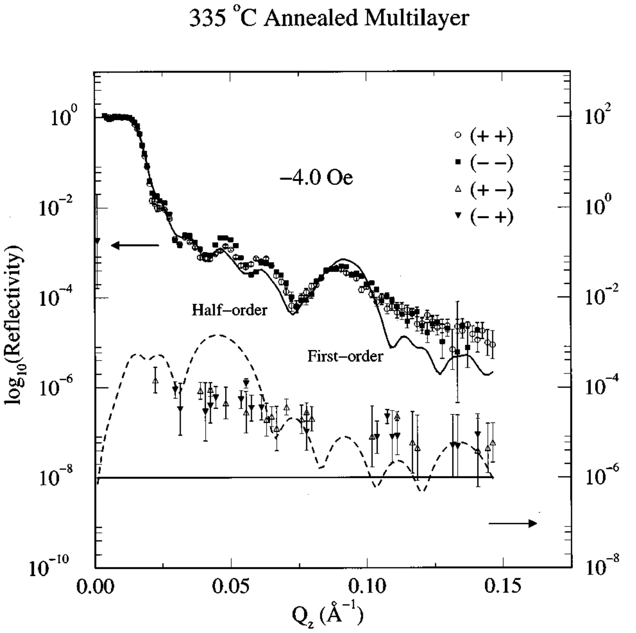

FIG. 8. Polarized neutron reflectivity for the 335 °C annealed sample prepared in a field of -4 Oe after saturation in a 150 Oe-field, in order to produce the demagnetized state. The circles and squares designate the $(++)$ and $(--)$ non-spin-flip cross sections, respectively, and the triangles and inverted triangles mark the $(+-)$ and $(-+)$ spin-flip cross sections, which are vertically offset by two orders of magnitude for clarity. (The arrows point to the appropriate vertical axis for each set of cross sections.) The solid lines correspond to a fit to the data, and the dashed line represents the scattering expected for antiferromagnetically aligned $\mathrm{Ni}_{80}\mathrm{Fe}_{20}$ layers with large in-plane domains assuming that the moments orient perpendicular to the applied field.

but after data correction we excluded all points that were negative or that had absolute values smaller than their estimated uncertainty.) A pronounced splitting is evident between the $(++)$ and $(--)$ intensities at both the critical angle and the first-order superlattice peak positions ($Q_z \approx 0.014$ and 0.090 Å^{-1}, respectively), while the $(+-)$ and $(-+)$ spin-flip intensities are effectively equal to background levels. We thus conclude that the sample magnetization is aligned parallel to the applied field direction as expected from the bulk magnetization measurements [Fig. 1(b)]. To reduce the number of variables in the fits to the data (solid and dashed lines in Fig. 7), we use the structural parameters[31] obtained from the analysis of the x-ray reflectivity data (Table I) as a guide and scale the neutron scattering length densities Nb for bulk $\mathrm{Ni}_{80}\mathrm{Fe}_{20}$ and Ag (9.13×10^{-6} and 3.47×10^{-6} Å^{-1}, respectively) to the fitted x-ray densities in order to account for the interlayer mixing. This analysis gives a $\mathrm{Ni}_{80}\mathrm{Fe}_{20}$ moment consistent with the bulk saturation value of $0.9\mu_B$, but the sensitivity of this fit is limited due to the extensive mixing of the $\mathrm{Ni}_{80}\mathrm{Fe}_{20}$ and Ag layers (Fig. 4) and due to the broadening of the first-order superlattice peak relative to the x-ray data, resulting from a distribution of bilayer thicknesses across the sample surface.[31] The principal effect of lowering the field below ≈ 10 Oe after saturation is to decrease the difference between the $(++)$ and $(--)$ superlattice peak intensities, implying a reduction of the projection of the moment parallel to the applied field.

We next probed the nature of the magnetic order for the 335 °C annealed multilayer in the zero-moment state obtained by setting the field to -4 Oe after saturation, as shown in Fig. 8. The applied field for this PNR scan was carefully selected to equal the measured coercive field of the sample, which is marked by an arrow on the hysteresis loop in Fig. 1(b). In contrast to the high-field neutron data in Fig. 7, the $(++)$ and $(--)$ intensities in Fig. 8 are essentially equal, though the $(+-)$ and $(-+)$ intensities remain indistinguishable from background. Surprisingly, *none* of the observed scattering is magnetic according to Eqs. (3) and (4). Data obtained for the as-deposited sample near $H_c = 0.6$ Oe [Fig. 1(a)] have nearly identical characteristics.

These measurements help us to eliminate the most obvious possibilities for the structure of the demagnetized spin state. In related GMR multilayers such as Fe/Cr, Co/Ru, and Co/Cu, neutron scattering measurements showed that the zero-field peak in the resistivity is associated with an antiparallel alignment along the growth axis of the ferromagnetic layer moments, which order in large in-plane domains.[32–34] If the moments orient perpendicular to the applied field within the sample plane, such a spin structure would give rise to the spin-flip scattering (illustrated by the dashed line in Fig. 8), which has a strong peak at the half-order position ($Q_z = 2\pi/2\Lambda \approx 0.045$ Å^{-1}). Relative to the 250 Oe reflectivity data (Fig. 7), no pronounced features emerge at half-order in *either* the non-spin-flip or spin-flip data upon lowering the

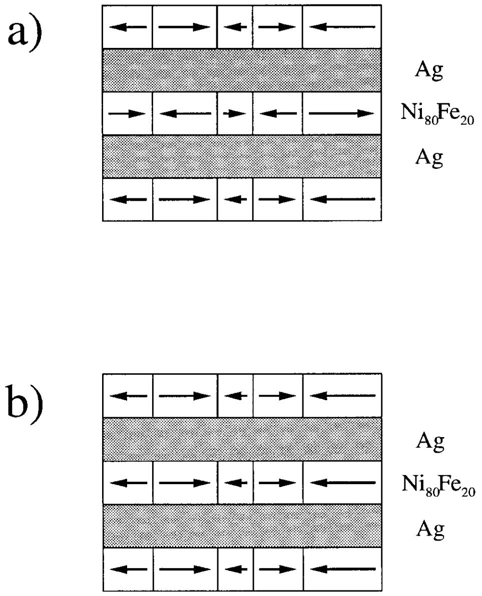

FIG. 9. (a) Idealized schematic of a proposed spin structure with the $Ni_{80}Fe_{20}$ moments aligned in in-plane domains that are correlated antiferromagnetically across the Ag layers along the growth-axis direction. In a real material the moments may be randomly oriented within the growth plane and the domain size may vary from one bilayer to the next. (b) Alternate spin structure with discrete in-plane domains that are correlated ferromagnetically along the growth axis.

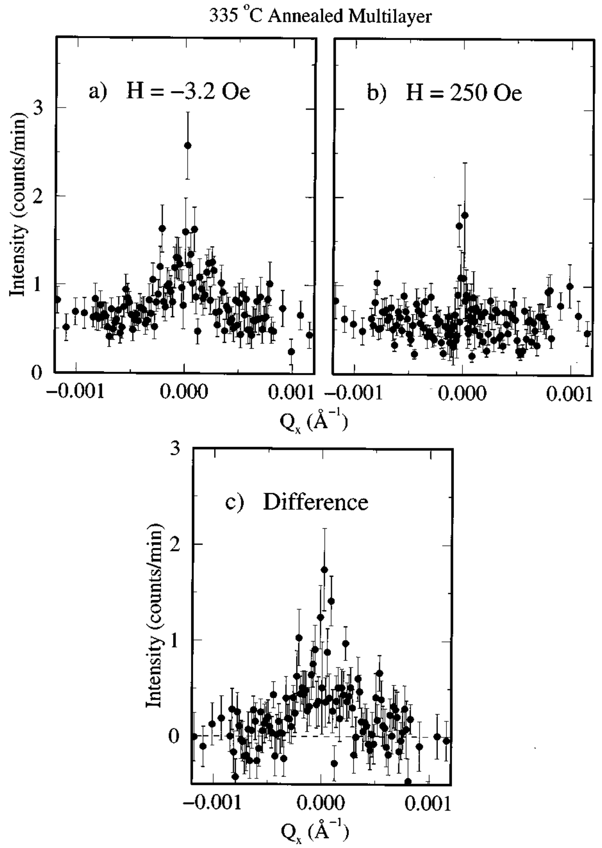

FIG. 10. Transverse neutron Q_x scans at the half-order antiferromagnetic position ($Q_z = 0.048$ Å^{-1}) for the 335 °C annealed multilayer prepared in fields of (a) −3.2 Oe to produce the demagnetized state and (b) 250 Oe to produce the saturated state. The data represent an addition of the (+ −) and (− +) cross sections and have been corrected for polarization efficiencies. The data shown in (c) are a subtraction of the 250 Oe data in (b) from the −3.2 Oe data in (a).

applied field, indicating that the 335 °C annealed multilayer does not order as a simple antiferromagnet like other GMR materials.

Other possible spin structures include ones with the orientation of the moments perpendicular to the sample plane, antiferromagnetically or ferromagnetically correlated $Ni_{80}Fe_{20}$ layers with the moments aligned in discrete in-plane domains, and random alignment of the in-plane domains across the intervening Ag. Figures 9(a) and 9(b), respectively, show simplified schematics of the antiferromagnetically and ferromagnetically correlated spin structures. It is unlikely that the spins align perpendicular to the plane in light of magnetization data that indicate that the easy axis of magnetization is in-plane.[11] Specular neutron reflectivity cannot distinguish among the other alternatives, however, because it averages over the in-plane magnetic structure if the domains are sufficiently small ($\lesssim$50–100 μm).

As discussed within the context of x-ray diffraction in Sec. III, transverse-Q_x scans [Fig. 2(a)] are sensitive to characteristics of the in-plane structure. The use of spin-polarization analysis helps to distinguish between those features associated with the magnetic versus the structural disorder. We have performed these measurements for the 335 °C annealed and as-deposited multilayers at Q_z values corresponding to the half- and first-order superlattice peak positions. Antiferromagnetic interlayer correlations along the z axis [Fig. 9(a)] will give rise to diffuse scattering at the half-order position, while ferromagnetic correlations [Fig. 9(b)] will produce scattering at the first-order position. We first examined each multilayer in its fully magnetized state ($H = 250$ Oe) in order to characterize the background resulting from both the instrument and the sample. Following this measurement, we slowly lowered the field toward the coercive value, designated by the arrow in Fig. 1, while monitoring the (+ +) and (− −) intensities at the first-order superlattice peak position ($Q_z \approx 0.09$ Å^{-1}) until they converged (Fig. 8). This procedure ensured that the sample was prepared in the demagnetized state for subsequent transverse-Q_x measurements. In general these transverse measurements require extended count times (e.g., 2–3 days at each Q_z position) due to the limited signal originating from the spin disorder.

Figures 10(a) and 10(b) show transverse spin-flip scans at the half-order position for the 335 °C annealed sample in fields of −3.2 and 250 Oe, respectively. A subtraction of these two data sets [Fig. 10(c)] confirms that the zero-moment spin configuration gives rise to broad, diffuse scattering centered at $Q_x = 0.0$ Å^{-1}. [Although these data have been corrected for the efficiencies of the polarizing elements,[28] a small, sharp peak remains near $Q_x = 0.0$ Å^{-1} in Fig. 10(b) because of residual spin leakage.] A visual inspection of the (+ +) and (− −) scans at the half-order position reveals extra diffuse intensity in the −3.2 Oe data relative to the 250 Oe data, though it is partially masked by

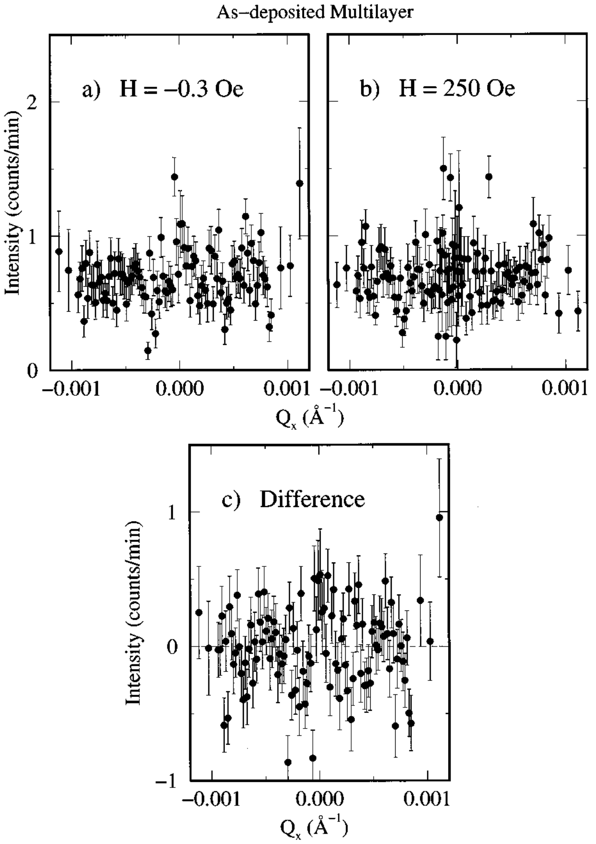

FIG. 11. Transverse neutron Q_x scans at the half-order antiferromagnetic position ($Q_z = 0.052$Å^{-1}) for the as-deposited multilayer prepared in fields of (a) -0.3 Oe to produce the demagnetized state and (b) 250 Oe to produce the saturated state. The data represent an addition of the $(+-)$ and $(-+)$ cross sections and have been corrected for polarization efficiencies. The data shown in (c) is a subtraction of the 250 Oe data in (b) from the -0.3 Oe data in (a).

a sharp specular peak of structural origin. By contrast, the spin-flip data obtained at the first-order position in a field of -3.2 Oe are indistinguishable from the 250 Oe data.[16] The diffuse scattering apparent in the first-order non-spin-flip data does not vary substantially with increasing field, though the intensity of the sharp specular peak changes as the $Ni_{80}Fe_{20}$ spins align ferromagnetically (Figs. 7 and 8). These results suggest that in the demagnetized state at least some portion of the moments within the nominal $Ni_{80}Fe_{20}$ layers are ordered in ferromagnetic domains with components both parallel and perpendicular to the applied field direction. These domains appear to be antialigned relative to each other across the intervening Ag, but the antiferromagnetic correlations are not long range judging by the absence of a distinct half-order peak in the total reflectivity data (i.e., scan equivalent to Fig. 8 prior to background subtraction). The presence of a small remanent moment in the magnetic hysteresis data for this sample, shown in Fig. 1(b), also suggests that a complete antiparallel alignment of the $Ni_{80}Fe_{20}$ layers is not achieved. The spin structure thus is of the character of that represented in Fig. 9(a).

As explained in Sec. III, the inverse of the FWHM of the diffuse scattering is related to the in-plane coherence length. Specifically, the transverse magnetic scattering may be broadened by both the uniform magnetization of interlayers with rough interfaces and the magnetic disorder resulting from in-plane domains.[18] The former has been characterized using off-specular x-ray measurements as described in Sec. III, and the width of the structural diffuse scattering near the half-order position ($Q_z = 0.05$ Å^{-1}) is approximately 1.0×10^{-4} Å^{-1} (Fig. 6). The width of the corresponding neutron peak in Fig. 10(a) is a factor of 3–6 times greater. The coherence length extracted from the width of the peak, which is entirely of magnetic origin [Eq. (4)], roughly corresponds to a magnetic domain size.[18,19] After fitting this peak to a Gaussian line shape and accounting for instrumental resolution, we approximate an average domain width of 1–5 μm, which is of the same order as the structural correlation length ξ (Sec. III). Only after improving the counting statistics can we refine this estimate using a more sophisticated theoretical formalism.[18]

The off-specular data obtained for the as-deposited multilayer indicate that the demagnetization proceeds by a different process. The spin-flip intensity at half-order measured in a field of -0.3 Oe [Fig. 11(a)] is indistinguishable from that measured in saturation [Fig. 11(b)], as demonstrated by the subtraction in Fig. 11(c). The same is true for the non-spin-flip scattering at the half-order position.[16] In fact, none of the transverse scans show *any* diffuse features when the field is lowered to its coercive value. By process of elimination, we conclude that in the zero-moment state the spins align in domains smaller than our detection limits. Thus we do not know if the $Ni_{80}Fe_{20}$ moments are systematically correlated relative to each other across the intervening Ag in a manner consistent with the spin structures depicted in Figs. 9(a) and 9(b).

V. INTERLAYER COUPLING MECHANISM

Both the neutron diffraction and bulk magnetization measurements [Fig. 1(a)] suggest that the coupling between the $Ni_{80}Fe_{20}$ layers in the as-deposited multilayer is weakly ferromagnetic, as has been observed in related studies.[14,35] It has been speculated[11] that this coupling results either from an intrinsic ferromagnetic exchange interaction mediated by the nonmagnetic Ag or from the presence of $Ni_{80}Fe_{20}$ ''pinholes'' which span Ag interlayers as thick as 45 Å.[35] Our data support the former interpretation, but we cannot completely rule out the latter because analysis of the specular x-ray data (Table I) indicates that both prior to and after annealing, trace amounts of $Ni_{80}Fe_{20}$ are dispersed throughout the nominal Ag layers (and vice versa). Locally, however, the laminar ordering is well defined (Fig. 3).

Upon closer examination of the fitted scattering densities, it seems that the $Ni_{80}Fe_{20}$ layers are strongly contaminated with Ag, though the Ag interlayers themselves are relatively pure. Within the sensitivity of our x-ray fits, the nature and extent of this interlayer mixing do not appear to vary with annealing temperature. On the other hand, complementary XTEM measurements[15] show evidence that Ag bridges form across the $Ni_{80}Fe_{20}$ interlayers as a result of annealing. Apparently the quantity of Ag in the $Ni_{80}Fe_{20}$ layers does not significantly increase upon annealing, but rather the Ag already present migrates and conglomerates, presumably near the grain boundaries. In addition, off-specular x-ray scans

(Fig. 5) reveal that the coherence length of the in-plane structural order increases systematically with annealing temperature. A picture of the annealing process emerges in which the Ag, Ni, and Fe atoms are mixed uniformly throughout the interfacial regions upon deposition, giving rise to short-range structural disorder. The in-plane coherence length increases after annealing as the Ag precipitates out of the $Ni_{80}Fe_{20}$ layers, forming ferromagnetic pancakes with reasonably flat interfaces. Though grain boundaries are not evident in Permalloy/Ag multilayers grown by molecular beam epitaxy,[14] a similar phase separation does occur in the preparation of $Ni_{80}Fe_{20}$ nanoparticles from sputtered alloy films[36] and from sputtered $Ni_{81}Fe_{19}$/Ag multilayers with ultrathin $Ni_{81}Fe_{19}$ layers.[37] Such a process could slightly enhance the magnetoresistance by lowering the resistivity associated with defect scattering and interfacial roughness,[14] as we observe.[11] (We note that this behavior contrasts with that of evaporated $Ni_{83}Fe_{17}$/Cu multilayers[38] which show an increase in both the GMR and the resistivity upon annealing. For these miscible materials, annealing promotes interfacial interdiffusion rather than phase separation, leading to an increase of the defect scattering.[39])

PNR measurements (Figs. 10 and 11) prove that the physical modifications of the multilayer that occur upon annealing also tend to induce an antiferromagnetic coupling and thus produce a more significant variation of the resistivity with applied field. Apparently, the Ag bridging of the $Ni_{80}Fe_{20}$ interlayers is accompanied by the formation of 1–5 μm in-plane magnetic domains. In related studies[11,17] it was suggested that the dipolar interaction, which favors antiparallel alignment of the $Ni_{80}Fe_{20}$ moments, is enhanced relative to the intrinsic ferromagnetic exchange as a result of this structural and magnetic reconfiguration. We demonstrate here that the field required to align two finite blocks of spins separated by a small distance s is, in fact, of the order of the saturation fields measured for the annealed $Ni_{80}Fe_{20}$/Ag multilayers ($\approx$50 Oe).

We begin by calculating the energy associated with the placement of a magnetized block with magnetization $\mathbf{M}_1$ in the presence of a field $\mathbf{B}_2=-\boldsymbol{\nabla}\Phi_2$ generated by another block with magnetization $\mathbf{M}_2$,

$$E=-\int_{V_1}\mathbf{M}_1\cdot\mathbf{B}_2 dV. \tag{5}$$

As shown in Fig. 12(a), it is assumed that $\mathbf{M}_1$ and $\mathbf{M}_2$ are aligned parallel to the y axis and have equal magnitude M. For simplicity we consider two blocks of equal height d, width W, and length L. Since only the magnetic flux through the ends of the block S_2^- and S_2^+ at $y_2=\pm L/2$ contributes substantially to the generated field, the magnetostatic potential Φ_2 can be approximated as

$$\Phi_2(\mathbf{r})=M\left[\int_{S_2^+}\frac{dx_2dz_2}{|\mathbf{r}-\mathbf{r}_{S_2^+}|}-\int_{S_2^-}\frac{dx_2dz_2}{|\mathbf{r}-\mathbf{r}_{S_2^-}|}\right], \tag{6}$$

where $\mathbf{r}_{S_2^-}=x_2\hat{\mathbf{x}}-(L/2)\hat{\mathbf{y}}+z_2\hat{\mathbf{z}}$ and $\mathbf{r}_{S_2^+}=x_2\hat{\mathbf{x}}+(L/2)\hat{\mathbf{y}}+z_2\hat{\mathbf{z}}$.

The field H_a required to align $\mathbf{M}_1$ and $\mathbf{M}_2$ is proportional to the energy difference between the parallel and antiparallel configurations,

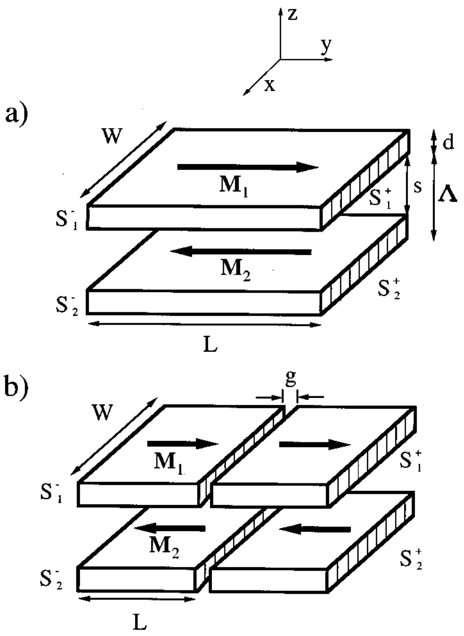

FIG. 12. (a) Schematic of two finite magnetic layers with moments $M_1=M_2$ to illustrate the geometry used for the calculation of the dipolar interaction. (b) Schematic of four finite magnetic slabs with a gap of width g introduced to simulate Ag structural inclusions through the $Ni_{80}Fe_{20}$ interlayers.

$$\begin{aligned}E_{\mathrm{diff}}&=2H_aMWLd\\&=2M\int_{V_1}\frac{\delta\Phi_2}{\delta y_2}dV.\end{aligned} \tag{7}$$

Substituting Eq. (6) into Eq. (7), we perform the integrals over x_1, x_2, z_1, and z_2 in the limit of $d,\Lambda\ll W,L$,

$$\begin{aligned}E_{\mathrm{diff}}=8M^2Wd^2\Bigg[&\frac{1}{2}-\frac{L}{W}+\sqrt{1+\frac{L^2}{W^2}}-\ln\left(\sqrt{1+\frac{W^2}{L^2}}+\frac{W}{L}\right)\\&+\frac{1}{2}\left(1+\frac{\Lambda}{d}\right)^2\ln\frac{2W}{\Lambda+d}+\frac{1}{2}\left(1-\frac{\Lambda}{d}\right)^2\ln\frac{2W}{s}\\&-\left(\frac{\Lambda}{d}\right)^2\ln\frac{2W}{\Lambda}\Bigg],\end{aligned} \tag{8}$$

where $\Lambda=d+s$ is the superlattice repeat distance. Combining Eqs. (7) and (8) for the case of $W=L$ (i.e., in plane magnetic domains with square sides), we derive an expression for the field H_a:

$$\begin{aligned}H_a=4M\frac{d}{W}\Bigg[&0.0328+\frac{1}{2}\left(1+\frac{\Lambda}{d}\right)^2\ln\frac{2W}{\Lambda+d}\\&+\frac{1}{2}\left(1-\frac{\Lambda}{d}\right)^2\ln\frac{2W}{s}-\left(\frac{\Lambda}{d}\right)^2\ln\frac{2W}{\Lambda}\Bigg].\end{aligned} \tag{9}$$

To simulate our $Ni_{80}Fe_{20}$/Ag multilayers, we plot $2H_a$ as a function of W in Fig. 13 with $d=20$ Å, $\Lambda=60$ Å, and $M=$ 760 emu/cm^3. In this calculation the alignment field is multiplied by an additional factor of 2 because each mag-

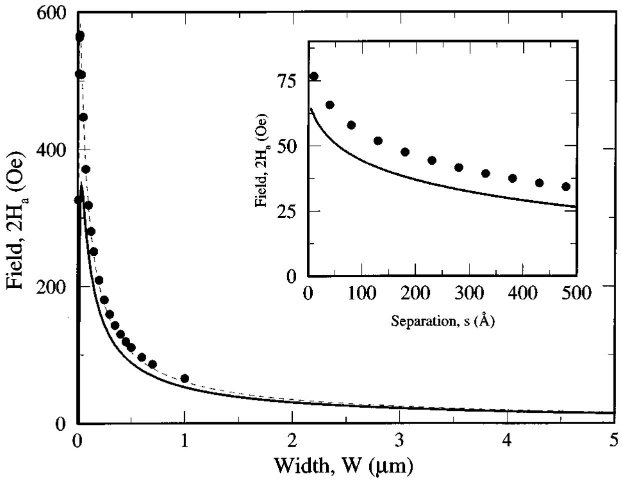

FIG. 13. Field $2H_a$ required to align stacked blocks of spins calculated as a function of the in-plane domain width W with $d = 20$ Å, $\Lambda = 60$ Å, and $M = 760$ emu/cm^3. It is assumed that the domain width and length are equal ($W = L$). In the inset the field is plotted as a function of the sheet separation distance s for $W = L = 1$ μm. The solid line represents the results of the approximate calculation outlined in the text, while the solid circles are the results of a direct summation assuming a perfectly cubic lattice. The dashed line corresponds to the calculation of the field required to align the same sheets of spins split in half by a 100 Å gap.

netic layer in an actual multilayer couples to two neighboring layers, rather than just one, assuming that the $x-y$ positions of the domain walls in each $Ni_{80}Fe_{20}$ layer are identical. In addition, the functional dependence of the alignment field on the separation between the layers is demonstrated in the inset of Fig. 13 for the case $W = L = 1$ μm. (We note that the results of this calculation are consistent with those from a more complex formalism described in Ref. 16 that is also valid in the limit of small d and Λ.)

In order to test this approximation, we have also calculated the alignment field directly by summing over the atomic point-dipole pairs.[40] Assuming that the atoms are arranged on a cubic lattice and that all $\mathbf{M}_{i,j}$ are equal and parallel to the y axis, the expression for the alignment field is written

$$H_a = \frac{M}{WLd} \sum_{i}^{V_1} \sum_{j}^{V_2} \frac{1}{|r_{i,j}|^3} - \frac{3y_{i,j}^2}{|r_{i,j}|^5}. \tag{10}$$

The geometrical dimensions of the blocks considered here are greatly limited by computer speed and memory size, but the points plotted in Fig. 13 illustrate that the integral approximation [Eq. (9)] converges with the exact calculation as the block width W approaches 1 μm.

From both approaches, it is evident that the magnitude of the alignment field gradually decays with increasing separation distance s and width W, which physically corresponds to the lateral dimension of the in-plane magnetic domains. Using the domain width of 1–5 μm measured for the 335 °C annealed sample, the calculated alignment field ranges from 60 to 14 Oe. Specifically, the measured saturation field of 50 Oe corresponds to an in-plane domain size of approximately 1.1 μm, according to Fig. 13. The alignment field would be reduced by the intrinsic ferromagnetic coupling, but a small, supplemental field may be required to align the in-plane domains.

An alternate model for the dipolar interaction in these multilayers has been proposed by Slonczewski.[17] Assuming that the in-plane magnetic domains extend to infinity, he neglects the magnetostatic contributions from the far ends of the dipole blocks (i.e., S_1^+ to S_2^+, S_1^- to S_2^-, S_1^+ to S_2^-, and S_1^- to S_2^+). Instead, a planar gap of width g parallel to the y axis of the magnetic slabs [Fig. 12(b)] is introduced to simulate the Ag structural bridges. The subsequent calculation of the interaction between the end surfaces of the four slabs in the gap region suggests that these Ag inclusions must be at least 10 Å wide to account for the measured saturation field.

Although the off-specular x-ray and neutron diffraction measurements imply that the structural grains are actually equal to or wider than the magnetic domains in annealed $Ni_{80}Fe_{20}$/Ag multilayers, we have modified our own model to include the unlikely presence of a single gap of width g in the center of two dipolar blocks [Fig. 12(b)]. Evaluating the integrals in the limit of $d,\Lambda \ll W,L$, the energy difference between the aligned and antialigned configuration is

$$\begin{aligned} E'_{\text{diff}} = 2E_{\text{diff}} + 8M^2Wd^2 \Bigg[& -\frac{1}{2} + \sqrt{1+4\frac{L^2}{W^2}} - 2\sqrt{1+\frac{L^2}{W^2}} - \ln(LW) + \ln\left(\frac{(W+\sqrt{W^2+L^2})^2}{W+\sqrt{W^2+4L^2}} \right) \\ & + \frac{g^2-\Lambda^2}{2d^2}\ln(\Lambda^2+g^2) + \frac{(\Lambda+d)^2-g^2}{4d^2}\ln[(\Lambda+d)^2+g^2] + \frac{s^2-g^2}{4d^2}\ln[(s^2+g^2)] - 2g\left(\frac{\Lambda}{d^2}\right)\tan^{-1}\left(\frac{\Lambda}{g}\right) \\ & + g\left(\frac{\Lambda+d}{d^2}\right)\tan^{-1}\left(\frac{\Lambda+d}{g}\right) + g\left(\frac{s}{d^2}\right)\tan^{-1}\left(\frac{s}{g}\right) \Bigg], \end{aligned} \tag{11}$$

where L now refers to the length of the structural grain. We note that the correction terms in this equation are similar to those derived by Slonczewski,[17] even though he only considers the case of $W=\infty$.

For a direct comparison with the simple two block case, we have calculated the alignment field ($2H_a$) from Eq. (11) with the assumption that the structural grain length L equals $W/2$. The plot in Fig. 13 demonstrates that the addition of a single structural gap tends to bolster the alignment field, though the gap must be wider than 100 Å in order to increase the field by as little as 6 Oe. Clearly the strength of the magnetostatic interaction is determined by the coupling between the far ends of the finite magnetic blocks (i.e., at the domain walls), rather than by the coupling across the gap.

In general, all of these calculations illustrate that the applied field required to overcome the dipolar interaction between stacked magnetic slabs with lateral dimensions of 1–5 μm is of the same order of magnitude as the saturation field measured for the $Ni_{80}Fe_{20}$/Ag multilayer annealed at 335 °C. In agreement with previous speculation,[11] we believe that the magnetostatic interactions, which favor antiparallel alignment of the interlayer moments, dominate the interlayer coupling after annealing. Apparently the emergence of flat $Ni_{80}Fe_{20}$ particles separated by Ag columns during the annealing process promotes magnetic domain wall formation within the sample plane. The dipolar coupling between these magnetic domains would be further enhanced by the presence of one or more of these Ag bridges within a single domain, as proposed by Slonczewski.[17]

VI. CONCLUSION

We have examined a series of annealed $Ni_{80}Fe_{20}$/Ag multilayers using x-ray and polarized neutron reflectivity techniques in an effort to understand the mechanism responsible for the enhanced field sensitivity of the GMR. Depth profiles of the sample composition, averaged across the sample plane, were extracted from specular x-ray measurements. This analysis indicates that the $Ni_{80}Fe_{20}$ and Ag interlayers are strongly mixed both prior to and after annealing, although more Ag is present in the nominal $Ni_{80}Fe_{20}$ layers, than $Ni_{80}Fe_{20}$ in the nominal Ag layers. Off-specular x-ray scans reveal that the apparent mixing arises from micrometer-scale features in the growth plane, such as terracing or grain boundaries, and that this planar disorder is effectively reproduced from one interface to the next (i.e., the roughness is conformal). Annealing up to 335 °C improves the local layering and increases the interfacial ‘‘flatness.’’ We propose that the Ag present within each $Ni_{80}Fe_{20}$ layer tends to precipitate out upon annealing and forms distinct bridges connecting adjacent Ag layers, possibly at grain boundaries, as suggested by complementary XTEM analysis.[15]

Polarized neutron reflectivity experiments indicate that the magnetic structure of the multilayers associated with the maximum GMR is more complex than the simple, single-domain antiferromagnetic order generally observed in related transition-metal materials. For samples annealed at 335 °C, the $Ni_{80}Fe_{20}$ moments in the demagnetized state align in plane in micrometer-sized domains that are oriented antiparallel along the growth axis across the intervening Ag layers. In transverse-Q_x scans through the half-order peak position, these domains give rise to a broad magnetic peak that is absent in comparable scans for the as-deposited multilayer. The presence of Ag inclusions within the $Ni_{80}Fe_{20}$ interlayers of the annealed samples clearly stabilizes magnetic domain wall formation.

An approximate calculation of the field required to align two finite slabs with uniform magnetization demonstrates that the antiparallel alignment of the $Ni_{80}Fe_{20}$ in-plane magnetic domains probably originates from dipolar coupling. For a stack of square blocks with side lengths ranging from 1 to 5 μm, we estimate the dipolar field to be 60–14 Oe, which is of the same order of magnitude as the saturation field measured for the 335 °C annealed multilayer. We suggest that the dipolar energy becomes sufficiently large to overcome intrinsic ferromagnetic exchange coupling following the formation of micrometer-order domains in the sample plane as a result of annealing. The resultant antiferromagnetic correlations among these domains give rise to anomalous GMR with high field sensitivity.

The fabrication of annealed $Ni_{80}Fe_{20}$/Ag multilayers[11] represents an innovative direction in the investigation of magnetoresistive materials that combines the best features of granular alloy films and transition-metal multilayers. Our studies continue in an attempt to provide a detailed analysis of the off-specular x-ray and neutron reflectivity data, which should illuminate the exact relationship between the structural grain boundaries and magnetic domain formation. Knowledge of the nature and origin of the magnetic structure in these materials obtained via neutron diffraction methods should enhance our ability to exploit this new technology for magnetic sensor applications.

ACKNOWLEDGMENTS

We would like to thank David Wiesler and Huai Zhang for useful discussions and insight regarding the interpretation of the off-specular scattering data.

---

*Current address: Microunity Systems Engineering, Inc., 255 Caspian Drive, Sunnyvale, CA 94089.

[1] M.N. Baibich, J.M. Broto, A. Fert, F. Nguyen Van Dau, F. Petroff, P. Eitenne, G. Creuzet, A. Friederich, and J. Chazelas, Phys. Rev. Lett. **61**, 2472 (1988).

[2] For a review of early work in the field, see L.M. Falicov, Daniel T. Pierce, S.D. Bader, R. Gronsky, Kristl B. Hathaway, Herbert J. Hopster, David N. Lambeth, S.S.P. Parkin, Gary Prinz, Myron Salamon, Ivan K. Schuller, and R.H. Victora, J. Mater. Res. **5**, 1299 (1990).

[3] S.S.P. Parkin, Phys. Rev. Lett. **67**, 3598 (1991).

[4] S.S.P. Parkin, R. Ghadra, and K.P. Roche, Phys. Rev. Lett. **66**, 2152 (1991).

[5] Eric E. Fullerton, M.J. Conover, J.E. Mattson, C.H. Sowers, and S.D. Bader, Appl. Phys. Lett. **63**, 1699 (1993); Phys. Rev. B **48**, 15 755 (1993).

[6] A.E. Berkowitz, J.R. Mitchell, M.J. Carey, A.P. Young, S. Zhang, F.E. Spada, F.T. Parker, A. Hutten, and G. Thomas, Phys. Rev. Lett. **68**, 3745 (1992).

[7] J.Q. Xiao, J.S. Jiang, and C.L. Chien, Phys. Rev. Lett. **68**, 3749 (1992).

[8] B. Dieny, V.S. Speriosu, S.S.P. Parkin, B.A. Gurney, D.R. Wilhoit, and D. Mauri, Phys. Rev. B **43**, 1297 (1991).

[9] S.S.P. Parkin, Phys. Rev. Lett. **71**, 1641 (1993).

[10] Thomas C. Anthony, James A. Brug, and Shufeng Zhang, IEEE Trans. Magn. **30**, 3819 (1994).

[11] T.L. Hylton, K.R. Coffey, M.A. Parker, and J.K. Howard, Science **261**, 1021 (1993); J. Appl. Phys. **75**, 7058 (1994).

[12] T.L. Hylton, Appl. Phys. Lett. **62**, 2431 (1993).

[13] B. Rodmacq, A. Mallon, and Ph. Gerard, in *Magnetic Ultrathin Films*, edited by B.T. Jonker, Takeshi Egami, Scott A. Chambers, P. Grünberg, R.F.C. Farrow, Kannan M. Krishnan, C. Chappert, Ernesto E. Marinero, R. Clarke, Carl Rau, W.J.M. de Jonge, and Shigeru Tsunashima, MRS Symposia Proceedings No. **313** (Materials Research Society, Pittsburgh, 1993), p. 185.

[14] R.F.C. Farrow, R.F. Marks, T.A. Rabedeau, M.F. Toney, D. Dobbertin, R. Beyers, and S.S.P. Parkin, J. Appl. Phys. **76**, 3688 (1994).

[15] M.A. Parker, T.L. Hylton, K.R. Coffey, and J.K. Howard, J. Appl. Phys. **75**, 6382 (1994).

[16] J.A. Borchers, P.M. Gehring, R.W. Erwin, C.F. Majkrzak, J.F. Ankner, T.L. Hylton, K.R. Coffey, M.A. Parker, and J.K. Howard, J. Appl. Phys. **79**, 4762 (1996); J.A. Borchers, P.M. Gehring, C.F. Majkrzak, J.F. Ankner, T.L. Hylton, K.R. Coffey, M.A. Parker, and J.K. Howard, in *Neutron Scattering in Materials Science*, edited by D.A. Neumann, T.P. Russell, and B.J. Wuensch, MRS Symposia Proceedings No. **376** (Materials Research Society, Pittsburgh, 1995), p. 577.

[17] J.C. Slonczewski, J. Magn. Magn. Mater. **129**, L123 (1994).

[18] Sunil K. Sinha, in *Neutron Scattering in Materials Science*, edited by D.A. Neumann, T.P. Russell, and B.J. Wuensch, MRS Symposia Proceedings No. **376** (Materials Research Society, Pittsburgh, 1995), p. 175.

[19] W. Hahn, M. Loewenhaupt, G.P. Felcher, Y.Y. Huang, and S.S.P. Parkin, J. Appl. Phys. **75**, 3564 (1994); J.E. Mattson, Eric E. Fullerton, C.H. Sowers, Y.Y. Huang, G.P. Felcher, and S.D. Bader, *ibid.* **73**, 5969 (1993).

[20] J. Takeda, Y. Endoh, H. Yasuda, K. Yamada, A. Kamijo, and J. Mizuki, J. Phys. Soc. Jpn. **62**, 3015 (1993).

[21] S.K. Sinha, J. Phys. (France) III **4**, 1543 (1994); S.K. Sinha, E.B. Sirota, S. Garoff, and H.B. Stanley, Phys. Rev. **38**, 2297 (1988).

[22] D.E. Savage, J. Kleiner, N. Schimke, Y.-H. Phang, T. Jankowski, J. Jacobs, R. Kariotis, and M.G. Lagally, J. Appl. Phys. **69**, 1411 (1991).

[23] A.P. Payne and B.M. Clemens, Phys. Rev. B **47**, 2289 (1993).

[24] Eric E. Fullerton, J. Pearson, C.H. Sowers, S.D. Bader, X.Z. Wu, and S.K. Sinha, Phys. Rev. B **48**, 17 432 (1993).

[25] J.F. Ankner and C.F. Majkrzak, in *Neutron Optical Devices and Applications*, edited by C.F. Majkrzak and J.L. Wood, SPIE Conf. Proc. No. 1738 (SPIE, Bellingham, WA, 1992), p. 260.

[26] V. Holý and T. Baumbach, Phys. Rev. B **49**, 10 668 (1994).

[27] J.-P. Schlomka, M. Tolan, L. Schwalowsky, O.H. Seeck, J. Stettner, and W. Press, Phys. Rev. B **51**, 2311 (1995).

[28] C.F. Majkrzak, in *Handbook of Neutron Scattering*, edited by W. Glaser (Springer-Verlag, Berlin, in press); Physica B **173**, 75 (1991).

[29] G.P. Felcher, Physica B **192**, 137 (1993); G.P. Felcher, R.O. Hilleke, R.K. Crawford, J. Haumann, R. Kleb, and G. Ostrowski, Rev. Sci. Instrum. **58**, 609 (1987).

[30] R.M. Moon, T. Riste, and W.C. Koehler, Phys. Rev. **181**, 920 (1960).

[31] The structural parameters (e.g., bilayer thickness) obtained from the neutron and x-ray reflectivity fits show subtle differences because the narrow x-ray beam is incident on only a small fraction of the sample, whereas the larger neutron beam completely bathes the sample. The neutron data thus tend to average over the structural inhomogeneities across the entire surface. In this case, the bilayer thickness near the sample's edges seem to differ from that in the center.

[32] A. Barthélémy, A. Fert, M.N. Baibich, S. Hadjoudj, F. Petroff, P. Etienne, R. Cabanel, S. Lequien, F. Nguyen Van Dau, and G. Creuzet, J. Appl. Phys. **67**, 5908 (1990).

[33] Y.Y. Huang, G.P. Felcher, and S.S.P. Parkin, J. Magn. Magn. Mater. **99**, L31 (1991).

[34] A. Schreyer, K. Bröhl, J.F. Ankner, C.F. Majkrzak, Th. Zeidler, P. Bödeker, N. Metoki, and H. Zabel, Phys. Rev. B **47**, 15 334 (1993).

[35] B. Dieny, V.S. Speriosu, S. Metin, S.S.P. Parkin, B.A. Gurney, P. Baumgart, and D.R. Wilhoit, J. Appl. Phys. **69**, 4774 (1991).

[36] M.A. Parker, K.R. Coffey, T.L. Hylton, and J.K. Howard, in *Magnetic Ultrathin Films*, edited by B.T. Jonker, Takeshi Egami, Scott A. Chambers, P. Grünberg, R.F.C. Farrow, Kannan M. Krishnan, C. Chappert, Ernesto E. Marinero, R. Clarke, Carl Rau, W.J.M. de Jonge, and Shigeru Tsunashima, MRS Symposia Proceedings No. 313 (Materials Research Society, Pittsburgh, 1993), p. 85.

[37] X. Bian, A. Zaluska, Z. Altounian, J.O. Ström-Olsen, Y. Huai, and R.W. Cochrane, in Ref. 36, p. 405.

[38] N. Smith, A. M. Zeltser, and M. R. Parker, IEEE Trans. Magn. **MAG-32**, 135 (1996); Alexander M. Zeltser and Neil Smith, J. Appl. Phys. **79**, 6254 (1996).

[39] V.S. Speriosu, J.P. Nozieres, B.A. Gurney, B. Dieny, H. Lefakis, T.C. Huang, and H. Lefakis, Phys. Rev. B **47**, 11 579 (1993).

[40] For example, Huai Zhang, J.W. Lynn, and D.E. Morris, Phys. Rev. B **45**, 10 022 (1992); Per Helvig Christensen and Steen Mørup, J. Magn. Magn. Mater. **35**, 130 (1983).